Formation, Thermal Stability and Mossbauer Effect of Amorphous, Quasicrystalline and Crystalline Phases in Al-(Cu, Ni)-Fe Systems

Formation, Thermal Stability and Mössbauer Effect of Amorphous, Quasicrystalline and Crystalline Phases in Al-(Cu, Ni)-Fe Systems *

An-Pang Tsai, Noriyuki Kataoka,
Akihisa Inoue and Tsuyoshi Masumoto
Institute for Materials Research

(Received January 30, 1992)

Synopsis

Nonequilibrium phase including amorphous and bcc phases in Al-Cu-Fe and Al-Ni-Fe systems formed by sputtering method. The composition range of the formation phases are determined, in harmony with that of the binary Al-transition system. The composition range (Ni=10~15 at%, Fe=10~15 at%) of melt-quenched quasicrystalline phase is the formation region of an amorphous phase in a vapor quenched state. In the investigation for $Al_{73}Ni_{10}Fe_{17}$ alloy, two exothermic peaks in calorimetric curves are observed during heating. The first peak is correlated with the precipitation of bcc-like nanocrystalline from vapor-quenched amorphous matrix, and the second peak is due to formation of decagonal phase. The Mössbauer spectra of these vapor-quenched nonequilibrium phases are examined and it is concluded that the local structure around Fe atom is similar among icosahedral, decagonal, amorphous and bcc phases.

I. Introduction

Shortly after the discovery[1] of the first icosahedral (i) phase in Al-Mn alloy, a series of newly discovered quasicrystal in Al-(Cu,Ni,Pd)-transition[2,3,4] metal(TM) have brought many aspects of interest in structure, stability and transport properties for theoretician and experimenter. As a result, a great progress of fundamen

---

* The 1882th report of Institute for Materials Research

tal understanding on quasicrystal have been achieved. In addition, such special samples have arise an essential problem of stability in quasicrystal, that is "what is the ground state of the quasicrystal?" This unresolved problem is giving rise a controversy among the proposed structural model of quasicrystal.

Structure and physical properties of the quasicrystals have been compared with amorphous and crystalline phases. Some similarities among the three phases have been proof and concluded that they have similar short range structure. Even though the structure of quasicrystal analogizes with that of amorphous and crystalline phases in different ways. It is known that a considerable amount of icosahedral clusters exist in amorphous phase. As the icosahedral cluster increase and connect to one another with the rule in sharing the face or the edge of icosahedron in quasicrystalline phase. On the other hand, some crystalline phases can be described as a three dimensional Penrose tiling quasicrystal with a fixed linear phason. Generally, such a crystalline phase have a giant lattice parameter. Indeed, the former is an ideal of "icosahedral glass"[5] and the later is an original conception of "approximant"[6] of quasicrystal, both described the frame structure of the quasicrystal.

By the way, the alloys prepared by the sputtering process may have additional non-equilibrium phase. It is also interesting that the comparison of the structure and physical properties among the non-equilibrium phases. We have found the amorphous, icosahedral, decagonal and bcc phases in Al-(Cu,Ni)-Fe alloys, having the composition close to another. In this report, we present the formation, thermal stability and Mössbauer effect of these phases.

II. Experimental Procedures

Master alloys and the targets for sputtering in the nominal composition were produced from high purity metal(Al,Ni,Cu,Fe) in Ar atmosphere using an arc furnace. An icosahedral Al-Cu-Fe and decagonal Al-Ni-Fe alloys were also fabricated for comparison. The film samples were prepared on polymide or copper substrate by a conventional rf sputtering method. The composition of the sputter-deposited films was determined by electron probe microanalysis (EPMA). The structure of the samples was confirmed by X-ray diffractometry. Thermal stability was examined by a differential scanning calorimetry (DSC).

III. Results and Discussion

1. Phase Formation in Al-Cu-Fe and Al-Ni-Fe Systems

Figure 1 shows the diffraction patterns of Al-Cu-Fe alloys prepared by sputtering. The as-sputtered phase is bcc phase with a lattice parameter of about 0.294 nm for $Al_{63}Cu_{23}Fe_{14}$, $Al_{66}Cu_{18}Fe_{16}$ and $Al_{70}Cu_{16}Fe_{14}$, amorphous phase for $Al_{71}Cu_{14}Fe_{15}$. While the melt quenched phase of these four alloys is an icosahedral phase.

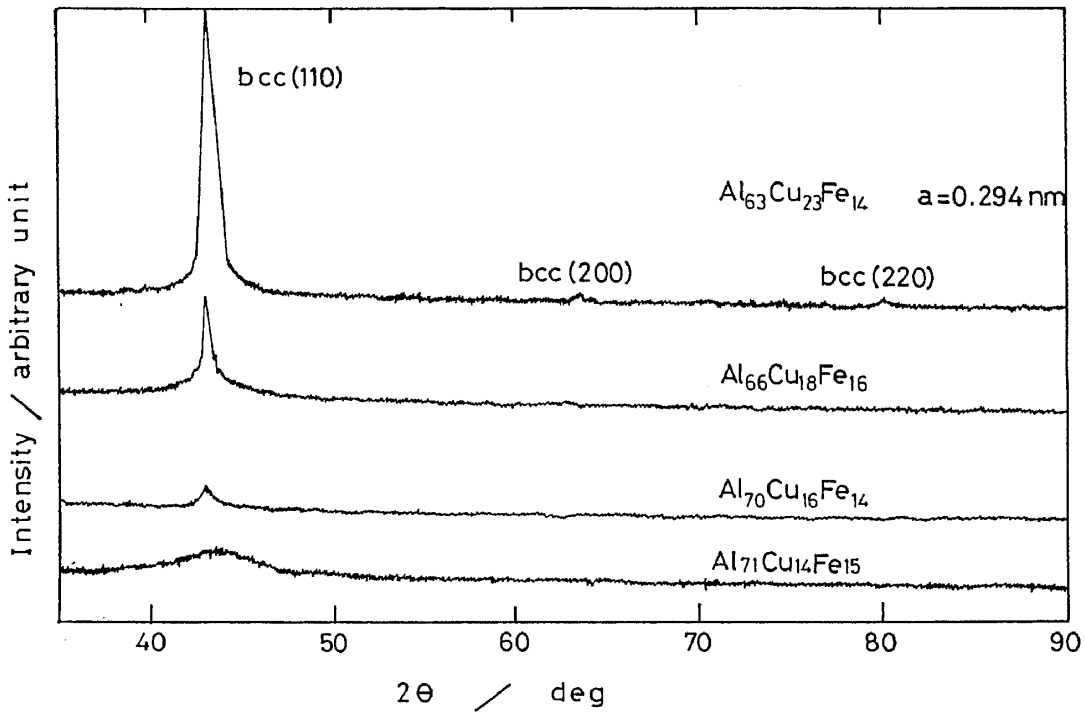

Fig.1 X-ray diffraction patterns of vapor quenched $Al_{63}Cu_{23}Fe_{14}$, $Al_{66}Cu_{18}Fe_{16}$, $Al_{70}Cu_{16}Fe_{14}$ and $Al_{71}Cu_{14}Fe_{15}$ alloys.

The phase formation prepared by sputtering are summarized in Fig. 2. We note that the bcc appears in the region of (Cu+Fe)>30at% and amorphous phase forms in a wide composition range from Al=90at%($Al_{90}Cu_5Fe_5$) to Al=65at%($Al_{65}Cu_{15}Fe_{20}$). The area surrounded by the broken line is the compositional range of the icosahedral(i-)[7] phase prepared by melt-quenching. It is the mixture of bcc and amorphous prepared by sputtering in the same range.

Figures 3 and 4 show the diffraction patterns of two alloy series in Al-Ni-Fe system. One is the alloy substituted Fe by Al (Fig. 3)

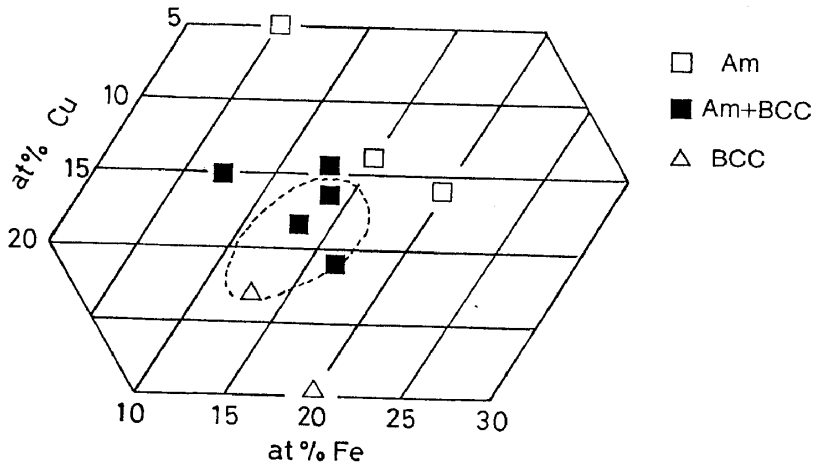

Fig.2 Phase diagram of Al-Cu-Fe ternary alloys prepared by vapor quenching method.

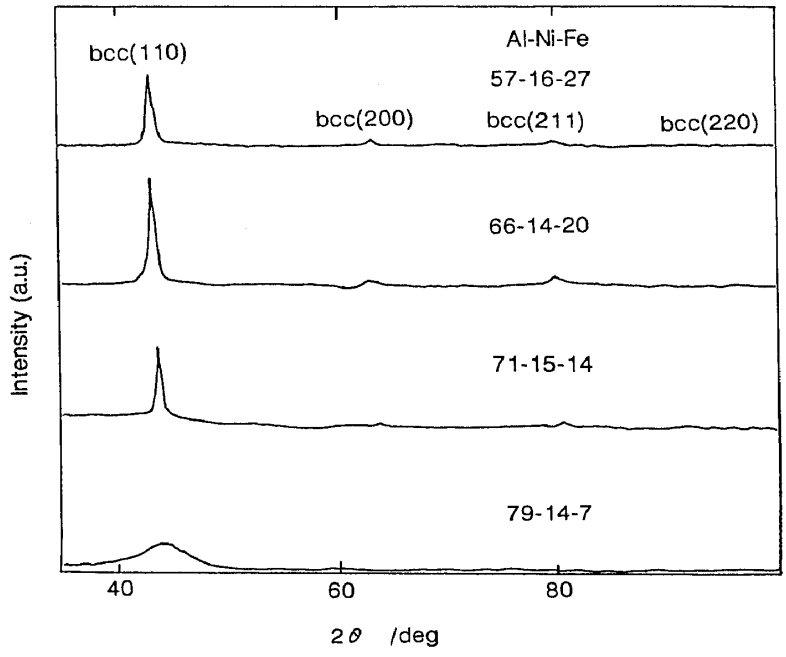

Fig.3 X-ray diffraction patterns of vapor quenched $Al_{57}Ni_{16}Fe_{27}$, $Al_{66}Ni_{14}Fe_{20}$, $Al_{71}Ni_{15}Fe_{14}$ and $Al_{79}Ni_{15}Fe_{14}$ alloys.

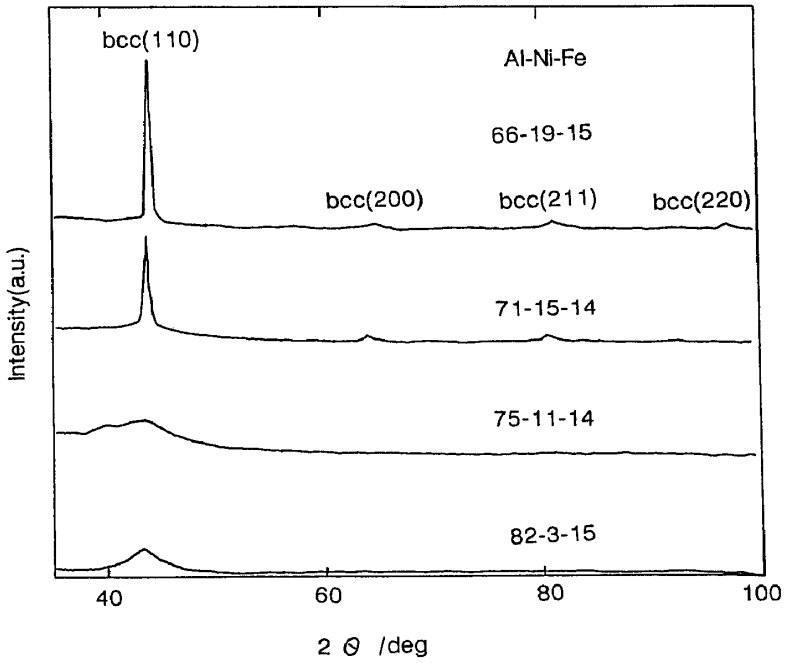

Fig.4 X-ray diffraction patterns of vapor quenched $Al_{66}Ni_{19}Fe_{15}$, $Al_{71}Ni_{15}Fe_{14}$, $Al_{75}Ni_{11}Fe_{14}$ and $Al_{82}Ni_3Fe_{15}$ alloys.

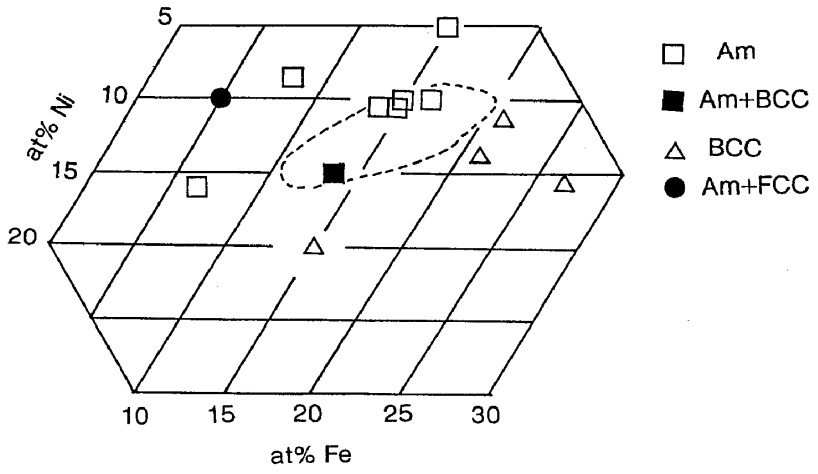

Fig.5 Phase diagram of Al-Ni-Fe ternary alloys prepared by vapor quenching method.

and the other is substituted Ni by Al (Fig.4). Amorphous phase appears in the Al-enriched region in both alloy series. The phase formation in Al-Ni-Fe alloys are summarized in Fig.5. As well as that in Al-Cu-Fe, the phase is the bcc in the region closed to $Al_{50}(Ni,Fe)_{50}$, amorphous phase in the region of Ni=10~15at% and Fe=10~15at% and fcc phase in the region of Ni<10at% and Fe<10at%. The region surrounded by broken line in Fig.5 represents the formation region of decagonal phase in liquid quenched state[8].

The formation of nonequilibrium phase by rf sputtering process in binary Al-transition metals(=Cr,Mn,Fe,Co,Ni) have been investigated. Some features are seen in the binary alloys; the amorphous phase forms at the compositions near Al=80at%, fcc phase appears as Al>80at% and the formation of bcc phase is in the region of Al<80 at%. The formation of amorphous phase in this limited composition range is attributed to be associated with the existence of complicated intermetallic compounds with a large lattice parameter more than 10 A and its unit cell is constructed by more than one hundred atoms, such as Al_7Cr, Al_4Mn, Al_3Ni, $Al_{13}Fe_4$ and $Al_{13}Co_4$[9,10]. The complication in structure of intermetallic compound is assumed to be in favor of the formation of amorphous phase. We noticed that the quaicrystal is formed in a melt-quenched state for the previously indicated binary intermetallic compounds. The tendency is the same in the present ternary Al-Ni-Fe and Al-Cu-Fe alloys, in which the sputtered-amorphous forms in the composition region of the formation of the melt-quenched quasicrystal. As a result, the formation range amorphous phase are wider for ternary alloys than binary alloys. Quasicrystal can be regarded as an intermetallic compound having a infinitely larger lattice parameter in other view. Thus, the present results is in compatible with the results in binary alloys.

2. Thermal Stability and Transformation in Al-Ni-Fe System

The DSC curves of the samples indicated in Fig. 5 are shown in Figs. 6,7 and 8. Some small exothermic peaks are seen (Fig.6) in bcc phase which containing higher Ni or Fe contents. The amorphous phase in Al-enriched ($Al_{80}Ni_8Fe_8$) area reveals one marked exothermic reaction with a heat flow of about 2.8 kJ/mole, while the amorphous phase containing 10~15 at%Ni and 10~15 at%Fe have similar feature that is crystallization occurs in two stage. The exothermic heat are about 0.84 kJ/mole for the lower temperature one and 1.27 kJ/Mole for the higher temperature one. We should remind that these alloys are a decagonal (D-) phase in a melt-quenched state and

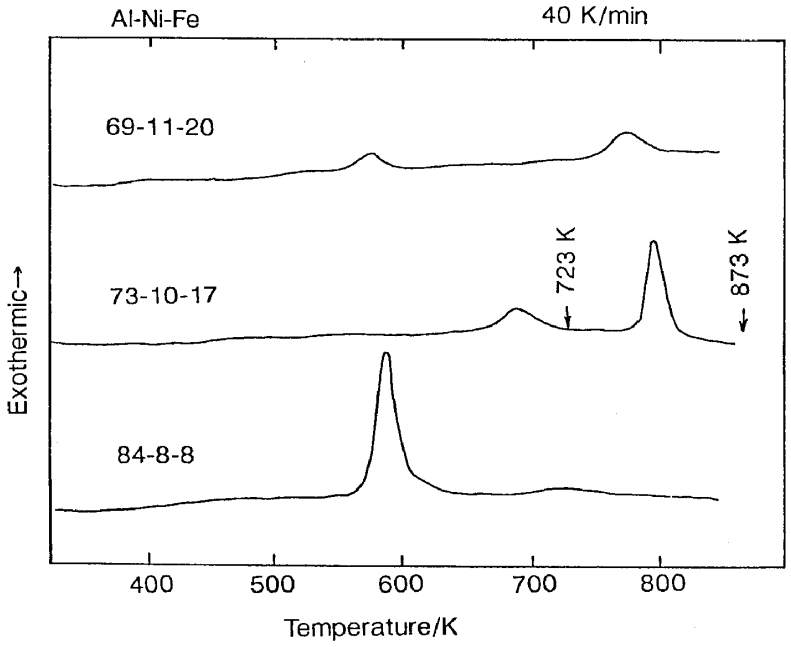

Fig.6 DSC curves of the vapor quenched $Al_{69}Ni_{11}Fe_{20}$, $Al_{73}Ni_{10}Fe_{17}$ and $Al_{84}Ni_8Fe_8$ alloys. The arrows indicate the heating temperature for transformation which shown in Fig. 9.

it is expected that the D-phase may occur after crystallization. Fig. 9 shows the X-ray diffraction (XRD) patterns of as sputtered $Al_{73}Ni_{10}Fe_{17}$ and after heated to 723 and 873 K which corresponding to the temperature after two transformation stage indicated in Fig.8, together with that of melt-quenched D-$Al_{75}Ni_{10}Fe_{15}$ for comparison. After heated over the first exothermic peak (723K) in DSC curve the weak diffraction peaks of bcc phase was dimly detected in XRD patterns (Fig.9(b)). When the sample heated to 873 K the full transformation is completed and the decagonal phase appears in XRD pattern. Thus, the lower temperature and higher temperature exothermic peaks in Fig. 8 corresponds respectively to the precipitation of bcc and formation of decagonal phase.

As described in Fig. 3, 4 and 5, the compositional range of melt-quenched decagonal phase locates between that of bcc (in higher (Ni+Fe) concentration) and Al-enriched amorphous phase. By taking composition distribution into account, we can presume that the first exothermic peak of $Al_{73}Ni_{10}Fe_{17}$ in DSC curves may be considered as a phase separation between Al-enriched amorphous and bcc phase (bcc

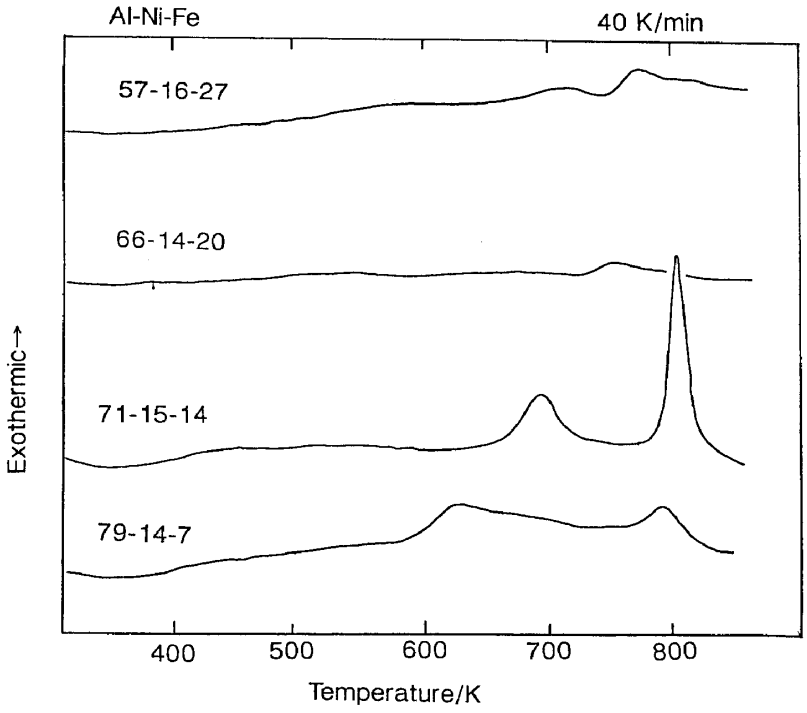

Fig.7 DSC curves of the vapor quenched $Al_{57}Ni_{16}Fe_{27}$, $Al_{66}Ni_{14}Fe_{20}$, $Al_{71}Ni_{15}Fe_{14}$ and $Al_{79}Ni_{14}Fe_{7}$ alloys.

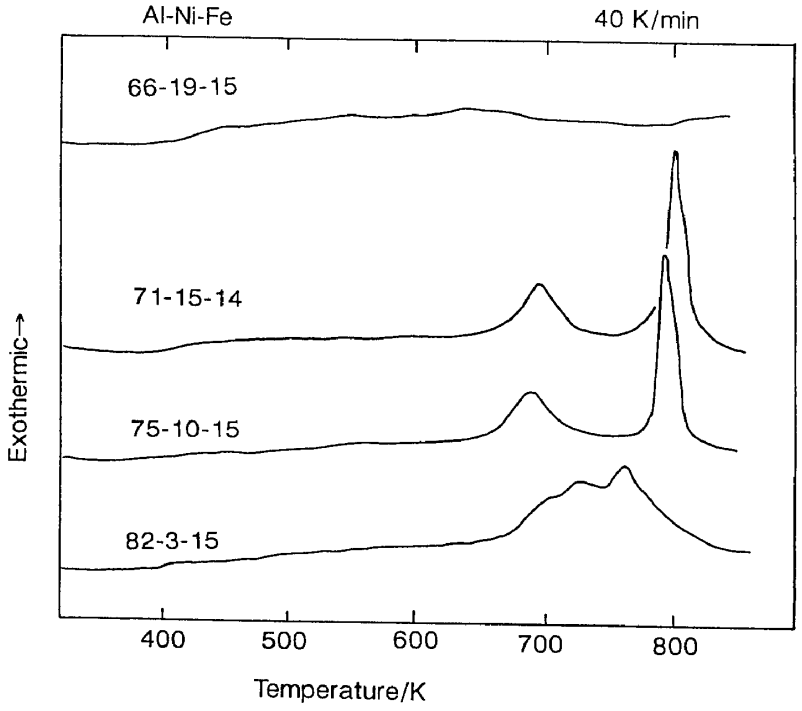

Fig.8 DSC curves of the vapor quenched $Al_{66}Ni_{19}Fe_{15}$, $Al_{71}Ni_{15}Fe_{14}$, $Al_{75}Ni_{10}Fe_{15}$ and $Al_{82}Ni_{3}Fe_{15}$ alloys.

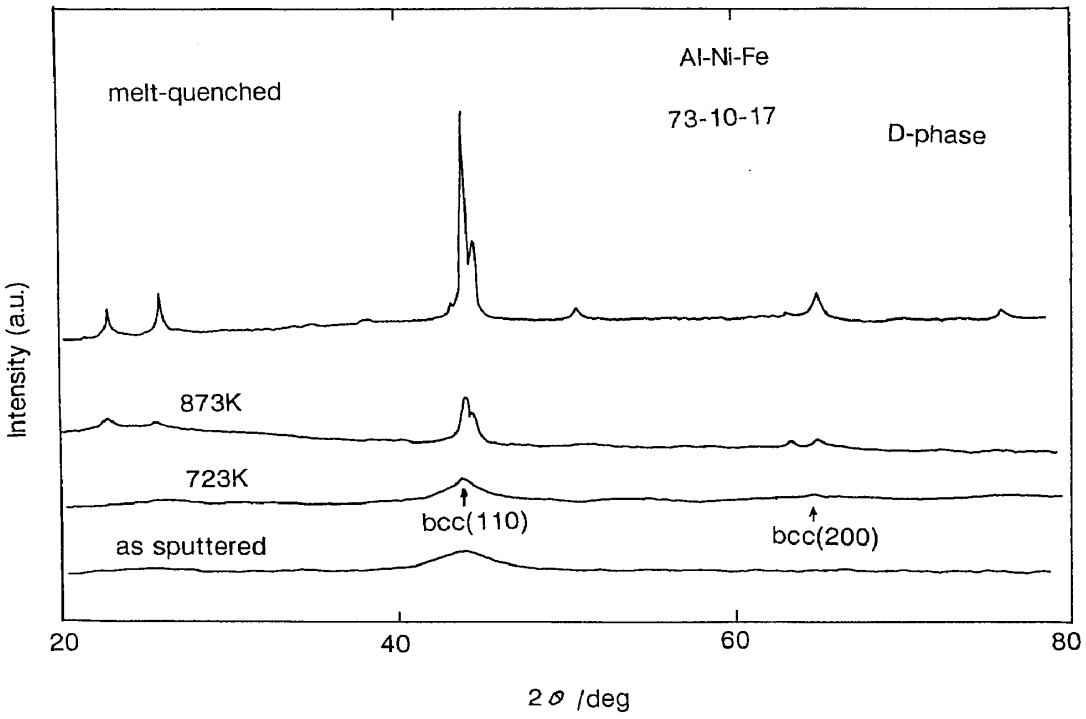

Fig.9 X-ray diffraction patterns for $Al_{73}Ni_{10}Fe_{13}$ alloy in as-sputtered state and heated to 723K and 873K respectively after sputtering, in comparison with that of melt-quenched state.

phase only formed at higher Ni and Fe concentration region), while the second exothermic peak is a solid-solid reaction between Al-enriched amorphous and bcc phases to a D-phase. The clear detail should be confirmed by transmission electron microscopic technique. Even though this speculation is quite reasonable and in a consistent with the result of solidification process that quasicrystal always forms through a peritectic reaction[11] between the bcc and Al-enriched melt. It has been clarified that all quasicrystal formed through a peritectic reaction in which the bcc phase acts as a nucleate site.

3. Mössbauer Effect

Figure 10 shows the Mössbauer spectra at 290K for melt-quenched icosahedral $Al_{65}Cu_{20}Fe_{15}$ (ICL), tetragonal $Al_7Cu_2Fe_1$ compound (TC),

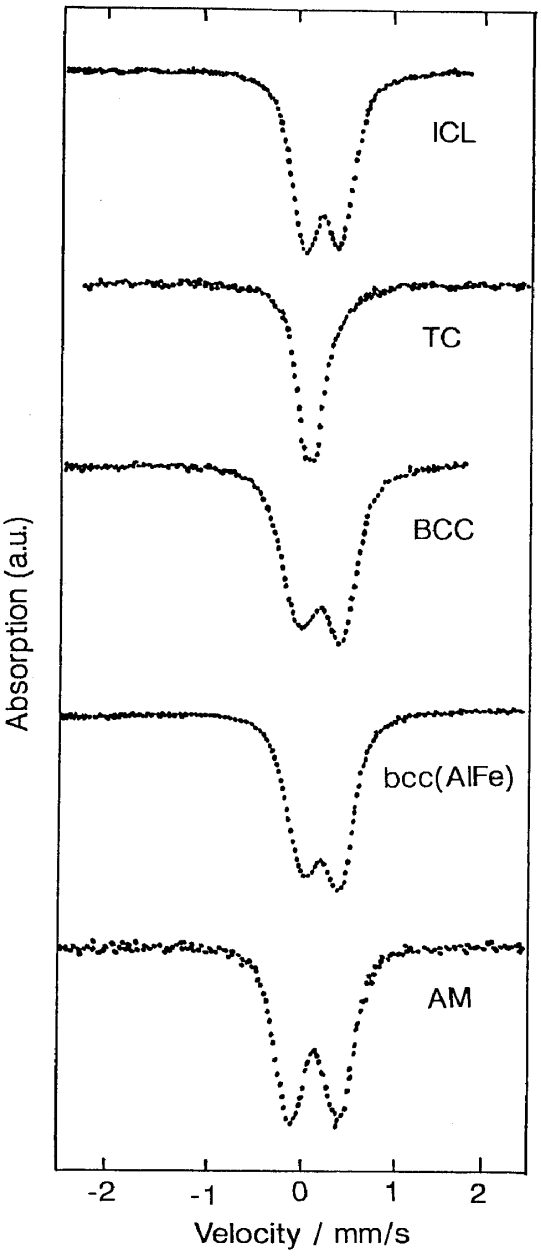

Fig.10 Mössbauer spectra at 290K for icosahedral $Al_{65}Cu_{20}Fe_{15}$(ICL), tetragonal $Al_7Cu_2Fe_1$ (TC), bcc $Al_{63}Cu_{23}Fe_{14}$ (BCC), bcc $Al_{62}Fe_{38}$ (bcc-AlFe) and amorphous $Al_{71}Cu_{14}Fe_{15}$. The velocity scale is relative to α-Fe at 290K.

TABLE 1. Average isomer shift, $\overline{IS}$, and average quadrupole splitting, $\overline{QS}$, as 290 K for ICA, TC, BCC and AM Al-Cu-Fe alloys. ICA, TC, BCC and AM are explained in the text.

	$\overline{IS}$ (mm/s)	$\overline{QS}$(mm/s)
ICA	0.23	0.47
TC	0.14	0.20
BCC	0.25	0.37
AM	0.22	0.42

the bcc $Al_{63}Cu_{23}Fe_{14}$ produced by sputtering (BCC), bcc $Al_{62}Fe_{38}$ (bcc-AlFe) and the amorphous phase prepared by vapor quenching (AM)[12]. Their spectra reveal a much wider linewidth of Mössbauer spectra than the nature width of ^{57}Fe. This phenomenon can be ascribed to a distribution of the electric field gradient. In order to fit broad spectrum , a linear relation between the isomer shift (IS) and quadrupole splitting (QS) was assumed. The average IS, $\overline{IS}$ and QS, $\overline{QS}$ for these phases are shown in table 1. The distribution curves of QS, P(QS), for the ICL, TC, BCC, bcc, and AM phases are shown in Fig. 11. Since an Fe has one crystallographic site with no Fe atom in its nearest neighbors for TC, small QS component are dominant for TC. Furthermore, the distribution curves of QS in Fig. 11 are similar for ICL, TC, BCC, bcc, and AM, although the QS value at maximum point of P(QS) for the AM is slightly larger than those of ICL, BCC and bcc; the zero QS component does not exist in the AM. This means that the electronic configurations around the Fe nuclei in are the same as those in the an Al-Fe compounds (bcc)[13].

The Mössbauer spectra of melt-quenched decagonal $Al_{75}Ni_{10}Fe_{15}$ (D), melt-quenched bcc $Al_{65}Ni_{20}Fe_{15}$ (BCC), bcc $Al_{62}Fe_{38}$ (bcc-AlFe) and vapor-quenched amorphous $Al_{75}Ni_{11}Fe_{14}$ (AM) are shown in Fig. 12[14]. Unlike that in Al-Cu-Fe system, the spectrum is different between decagonal, bcc and amorphous phases. While the values of isomer shifts (table 2) of these samples are in the same range as those of Al-Fe intermetallic compounds. It is noteworthy that the spectrum of the D-phase is analogous to that of the i-phase (in Fig. 10). These features imply that the electronic configurations around

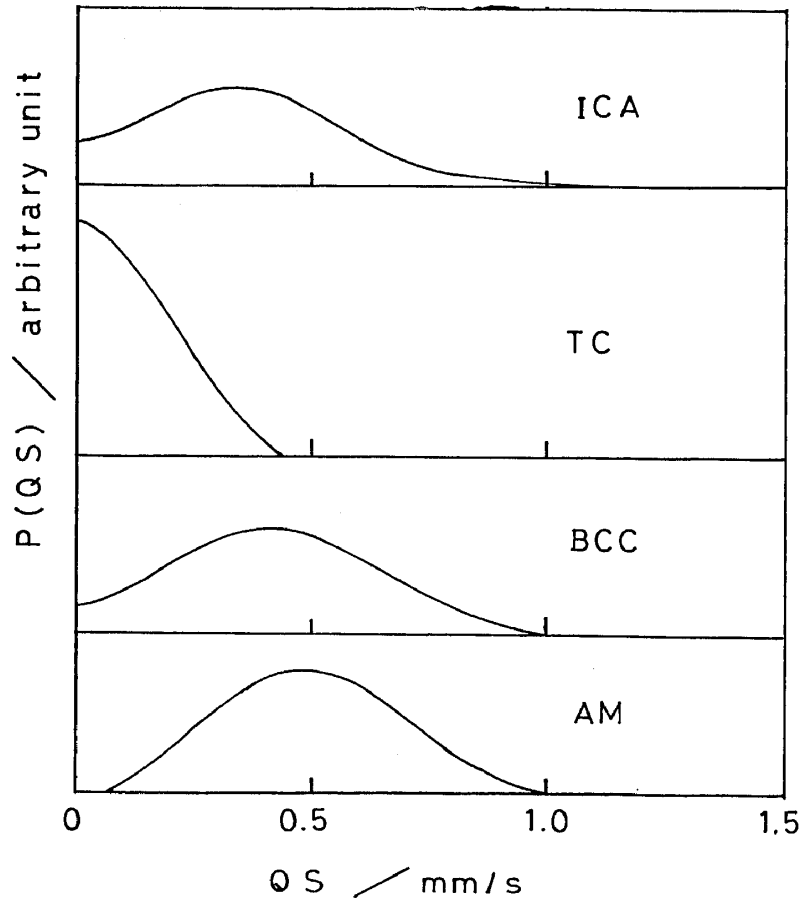

Fig.11 Distribution of quadrupole splitting, QS, for icosahedral $Al_{65}Cu_{20}Fe_{15}$ (ICL), tetragonal $Al_7Cu_2Fe_1$ (TC), bcc $Al_{63}Cu_{23}Fe_{14}$ (BCC), and amorphous $Al_{71}Cu_{14}Fe_{15}$.

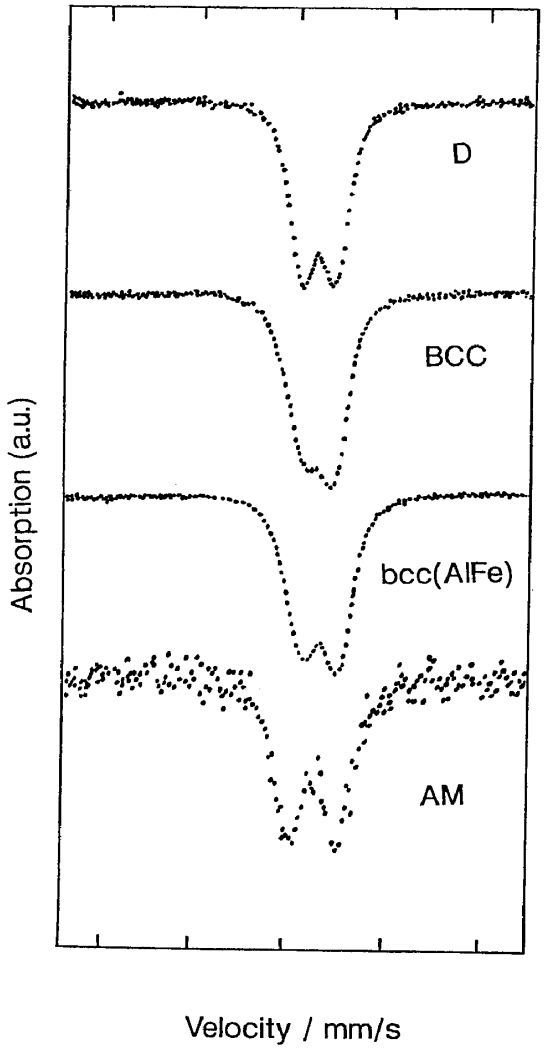

Fig.12 Mössbauer spectra at 290K for decagonal $Al_{75}Ni_{10}Fe_{15}$ (D), bcc $Al_{65}Ni_{20}Fe_{15}$ (BCC), bcc $Al_{62}Fe_{38}$ (bcc-AlFe) and amorphous $Al_{75}Ni_{11}Fe_{14}$ (AM).

TABLE 2.TABLE 2. Average isomer shift, $\overline{IS}$, and average quadrupolesplitting, $\overline{QS}$, as 290 K for D, BCC and AM Al-Ni-Fe alloys. D, BCC, and AM are explained in the text.

	$\overline{IS}$ (mm/s)	$\overline{QS}$(mm/s)
D	0.18	0.30
BCC	0.21	0.24
AM	0.22	0.42

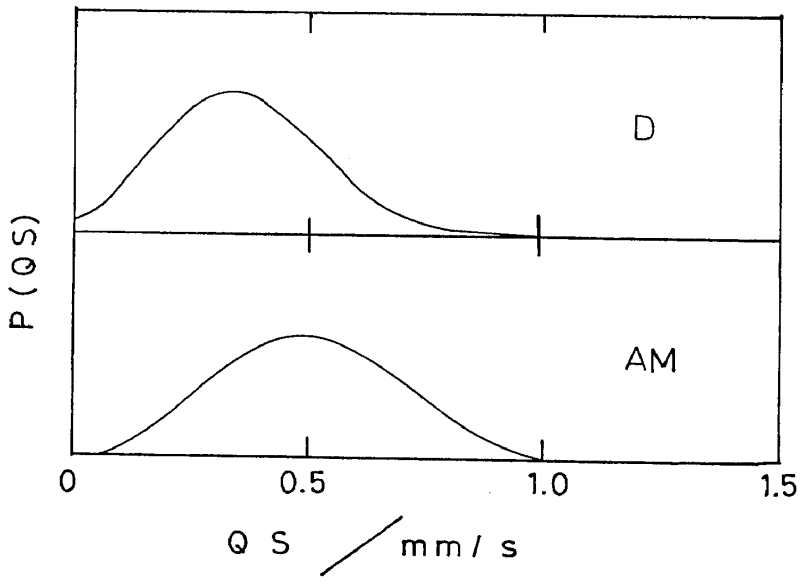

Fig.13 Distribution of quadrupole splitting,QS, for D-$Al_{75}Ni_{10}Fe_{15}$ and AM-$Al_{75}Ni_{11}Fe_{14}$.

the D- , i- and AM-phases are similar those in Al-Fe intermetallic compounds. The distribution curves of quadrupole splitting (QS-P(QS)) for the D- and AM-phases are shown in Fig. 13. The distribution curve of QS is similar for the D- ,and AM-phases, although the QS value at maximum point of P(QS) for the AM-phase is slightly larger than that of the D-phase. As well as the results for Al-Cu-Fe i-phase, the zero component does not exist for the AM in the present system. Combining the Mössbauer effect of these phase, we claim that the local structure around Fe atom is similar for i-, D-, AM and bcc phases.

In conclusion, we have prepared nonequilibrium phase including amorphous and bcc phases in Al-Cu-Fe and Al-Ni-Fe systems formed by vapor sputtered method. The composition range of the formation phases are determined. The bcc phase appears in the region of (Cu+Fe)>30at% and amorphous phase forms in the region from Al=90 at% to Al=65at% for Al-Cu-Fe system. The similar formation tendency is observed in Al-Ni-Fe system. The composition region(Ni=10~15 at%, Fe=10~15 at%) for quasicrystalline phase in a melt quenching state becomes to that of amorphous in a vapor quenched state. In this region, two exothermic peaks in calorimetric curves are observed during heating. The first peak is correlated with the precipitation of bcc-like nanocrystalline from vapor-quenched $Al_{73}Ni_{10}Fe_{17}$ amorphous matrix, and the second peak is due to formation of decagonal phase. The Mössbauer spectra of these vapor-quenched nonequilibrium phases are examined and it is concluded that the local structure around Fe atom is similar among icosahedral, decagonal,amorphous and bcc phases.

Acknowledgements

We wish to thank Dr. K. Sumiyama and Professor Y.Nakamura for their support in the Mössbauer effect measurement. We also wish to thank Mrs. K. Ohtera and K. Kita and J. Nagahora in Yoshida Kogyo K.K. for EPMA.

References

(1) D. Shechtman, I.A. Blech, D. Gratias and J.W. Cahn, Phys. Rev. Lett., 53 (1984), 1954.

(2) A.P. Tsai, A. Inoue and T. Masumoto, Jpn. J. Appl. Phys.

26,(1987), L1505.

(3) A.P. Tsai, A. Inoue and T. Masumoto, Mater.Trans., JIM., 30 (1989), 666.

(4) A.P. Tsai, Y. Yokoyama. A. Inoue and T, Masumoto, Jpn. J. Appl. Phys., 29 (1990), L11.

(5) P. Stephen and A.I. Goldman, Phy. Rev. Lett., 59 (1986), 1168 and 2331.

(6) C.L. Henley and V. Elser, Phil. Mag., B35 (1986), L59.

(7) A.P. Tsai, A. Inoue and T. Masumoto, J. Mater. Sci. Lett., 6 (1987), 1403.

(8) A.P. Tsai, A. Inoue and T. Masumoto, Mater. Trans., JIM., 30 (1989), 150.

(9) K. Masui, S. Maruno, S. Sakakibara and T. Kawaguchi, J. Non-Cryst. Solids, 74 (1985), 271.

(10) K. Masui, H. Nakamoto, S. Maruno, T. Kawaguchi and S. Sakaki bra, J. Non-Cryst. Solids, 124 (1990), 121.

(11) A.P. Tsai, Y. Yokoyama, A. Inoue and T. Masumoto, Proceeding on international symposium on the physics and chemistry of finite system, Richmond(1991).

(12) N. Kataoka, A.P. Tsai, A. Inoue and T. Masumoto, Jpn. J. Appl. Phys., 27 (1988), L1125.

(13) S. Nasu, U. Gonser and R.S. Preston, J. Phys. 41 (Paris) (1980), C1-385.

(14) A.P. Tsai, N. Kataoka, A. Inoue and T. Masumoto, Jpn. J. Appl. Phys. 29 (1990), L1696.